Submitted to ApJ. – DECEMBER 8, 2010
Preprint typeset using LaTeX style emulateapj v. 8/13/10

THE TWO PHASES OF GALAXY FORMATION

LUDWIG OSER[124], JEREMIAH P. OSTRIKER[3], THORSTEN NAAB[14], PETER H. JOHANSSON[1], ANDREAS BURKERT[1]
[1] Universitäts-Sternwarte München, Scheinerstr. 1, D-81679 München, Germany; oser@usm.lmu.de
[2] Max-Planck-Institut für extraterrestrische Physik, Giessenbachstrasse, D-85748 Garching, Germany
[3] Department of Astrophysical Sciences, Princeton University, Princeton, NJ 08544, USA
[4] Max-Planck-Institut für Astrophysik, Karl-Schwarzschild-Strasse 1, 85741 Garching, Germany
Submitted to ApJ. – *December 8, 2010*

ABSTRACT

Cosmological simulations of galaxy formation appear to show a 'two-phase' character with a rapid early phase at z$\gtrsim$2 during which 'in-situ' stars are formed within the galaxy from infalling cold gas followed by an extended phase since z$\lesssim$3 during which 'ex-situ' stars are primarily accreted. In the latter phase massive systems grow considerably in mass and radius by accretion of smaller satellite stellar systems formed at quite early times ($z > 3$) outside of the virial radius of the forming central galaxy. These tentative conclusions are obtained from high resolution re-simulations of 39 individual galaxies in a full cosmological context with present-day virial halo masses ranging from $7\times10^{11}M_{\odot}h^{-1} \lesssim M_{\rm vir} \lesssim 2.7\times10^{13}M_{\odot}h^{-1}$ (h=0.72) and central galaxy masses between $4.5\times10^{10}M_{\odot}h^{-1} \lesssim M_* \lesssim 3.6\times10^{11}M_{\odot}h^{-1}$. The simulations include the effects of a uniform UV background, radiative cooling, star formation and energetic feedback from SNII. The importance of stellar accretion increases with galaxy mass and towards lower redshift. In our simulations lower mass galaxies ($M_* \lesssim 9\times10^{10}M_{\odot}h^{-1}$) accrete about 60 per cent of their present-day stellar mass. High mass galaxy ($M_* \gtrsim 1.7\times10^{11}M_{\odot}h^{-1}$) assembly is dominated by accretion and merging with about 80 per cent of the stars added by the present-day. In general the simulated galaxies approximately double their mass since z=1. For massive systems this mass growth is not accompanied by significant star formation. The majority of the in-situ created stars is formed at $z > 2$, primarily out of cold gas flows. We recover the observational result of 'archaeological downsizing', where the most massive galaxies harbor the oldest stars. We find that this is not in contradiction with hierarchical structure formation. Most stars in the massive galaxies are formed early on in smaller structures, the galaxies themselves are assembled late.

Subject headings: cosmology: theory – dark matter – galaxies: evolution – galaxies: formation – methods: numerical

1. INTRODUCTION

Our understanding of galaxy formation has made great advances in the last two decades driven - primarily - by technological progress. Both ground and sky based measurements have allowed direct observation of various phases of galaxy formation and evolution over cosmic time with some detailed information now available at redshifts $z > 2$ (e.g. Steidel et al. 1999; Pettini et al. 2001; Genzel et al. 2006; Förster Schreiber et al. 2006; Trujillo et al. 2007; Kriek et al. 2008; van Dokkum et al. 2008; Marchesini et al. 2009; Förster Schreiber et al. 2009). Simultaneously with a quite definite cosmological model (ΛCDM, e.g. Spergel et al. 2007, Komatsu et al. 2010) having gained wide acceptance, we can, with increasing accuracy, simulate the evolution of galaxies from realistic initial conditions, with numerical resolution (in mass, space, and time) and physical modeling approaching the necessary degree of refinement (e.g. Sommer-Larsen et al. 2003; Springel & Hernquist 2003; Springel 2005; Nagamine et al. 2005; Naab et al. 2007; Governato et al. 2007; Piontek & Steinmetz 2009; Scannapieco et al. 2009; Sawala et al. 2010; Agertz et al. 2010; Schaye et al. 2010)

The overall results are reassuring, with simulations and observations agreeing - in gross outline - as to the time evolution of star/galaxy formation (e.g. Nagamine et al. 2006; Schaye et al. 2009) as well as the global attributes of the galaxies such as luminosity distribution and spatial organization (e.g. Cen & Ostriker 1999; Kauffmann et al. 1999; Somerville & Primack 1999; Springel et al. 2005; Kereš et al. 2009a; Guo et al. 2010a). Understanding the development of the internal structures of galaxies has been far more difficult to achieve with respect to the galactic stellar mass fractions (e.g. Kereš et al. 2009a; Guo et al. 2010b) as well as kinematics and morphologies (e.g. Abadi et al. 2003; Governato et al. 2010; Feldmann et al. 2010).

The terms with which we might usefully describe such development are still controversial (e.g. Meza et al. 2003; Naab et al. 2007; Governato et al. 2007; Piontek & Steinmetz 2009). In a hierarchically organized universe it has been natural to focus on overdense 'lumps' of dark matter gas or stars and to follow the merger history of these lumps. A recent paper by Hopkins et al. (2009) shows how useful this picture can be. But this is not the only description of galaxy formation. For example Kereš et al. (2005, 2009b) and Dekel et al. (2009b) have focused on how convergent cold streams of gas lead to early star bursts and the formation of the cores of massive galaxies. Naab et al. (2007, 2009), Joung et al. (2009) and others have used high resolution hydro simulations to explore this phase in greater detail (see also Meza et al. (2005) for the accretion histories of stellar halos of disk galaxies).

One fundamental and useful distinction is to examine if

a given star in the final galaxy was made (from gas) close to the center of the final system or, alternatively, near the center of some other, distant system and accreted in stellar form to the final galaxy. This distinction is useful, e.g. for understanding the size evolution of massive galaxies (Khochfar & Silk 2006a; Naab et al. 2007, 2009; Bezanson et al. 2009; Nipoti et al. 2009a; Hopkins et al. 2010; Feldmann et al. 2010). In the simulations presented here we find that most stellar particles in massive galaxies are formed at high redshift either far inside the virial radius ($\lesssim$ 3kpc) near the forming galaxy center or, alternatively in small systems outside the virial radius of the galaxy at a given cosmic time. We characterize the first category of stars as made 'in-situ' and the second as accreted or formed 'ex-situ'. In-situ stars are made (by definition) near to the galactic center over an extended time period. They are made from dissipative gas and, for massive systems, probably have relatively high metalicity (Zolotov et al. 2010). The peak rate of star formation for this category may be relatively early and in fact is very early ($z \approx 4$) for the most massive systems.

On the contrary, the accreted stars are typically made at quite early times as well, outside the virial radius, but added to the parent galaxy late in its evolution. They are added typically at radii larger than the effective radius, $r > r_{\rm eff}$, and are expected to be metal poor, since they originated in lower mass, lower metallicity systems (Naab et al. 2009). The ex-situ stars accrete via an energetically conservative process and their final binding energy is transferred to other phases (gas, stars, and dark matter) rather than simply radiated away (Johansson et al. 2009).

This alternative way of envisioning galaxy formation has many corollaries and makes many observed facts easier to understand. In massive systems we expect considerable growth in mass and radius at late times but little star formation, with the late forming stellar envelopes comprised of stars which are typically older than the stars in the bulk of the galaxy. Further we find systematic trends with galaxy mass. As one considers systems of lower mass, the in-situ component becomes increasingly dominant and the period of in-situ star formation is stretched out from being a small fraction of the Hubble time to a large fraction thereof.

The paper is organized as follows. In section 2 we describe our simulations in detail, as there will be follow-up papers using this set of simulations. In addition we here discuss the conversion efficiency of gas into stars for our simulated galaxies. In section 3 we examine the dependence of the ratio of in-situ formed to accreted stars on the galaxy stellar mass along with its implications. We go on to analyze the half-mass radii of the different stellar components of our simulated galaxies in section 4. Finally, in section 5 we summarize our findings.

2. SIMULATIONS

2.1. *The large-scale dark matter simulation*

To find candidate dark matter halos for later refinement we performed a dark matter only simulation of a cosmological volume with a comoving side length of $72\mathrm{Mpc\,h^{-1}}$ including 512^3 dark matter particles with individual masses of $m_p = 2 \times 10^8 M_\odot h^{-1}$. The box is large enough to provide a representative piece of the universe and the mass resolution fine enough to allow us to reliably find dark matter halos with $\sim 10^3$ particles being more massive than $\sim 10^{11} M_\odot h^{-1}$. The initial conditions were created using GRAFIC1 and LINGERS (Bertschinger 1995), assuming a ΛCDM cosmology with nearly scale-invariant initial adiabatic fluctuations. The cosmological parameters are based on the 3-year results from WMAP (Spergel et al. 2007) with σ_8=0.77, Ω_m=0.26, Ω_Λ=0.74, h = 0.72 ($\equiv H_0$=100h $\mathrm{kms^{-1}Mpc^{-1}}$) and the initial slope of the power spectrum is n_s=0.95. The initial conditions were then evolved from a redshift of $z \sim 43$ to $z = 0$ using GADGET-2 (Springel 2005) with a fixed comoving gravitational softening length of $2.52\mathrm{kpc\,h^{-1}}$. The simulation data was stored in 95 snapshots separated by $\Delta a = 0.01$ beginning at a cosmological expansion factor of a=0.06 ($z \approx 43$).

At z=0 we identify halos with a friends-of-friends algorithm and determine their centers using the shrinking sphere technique (Power et al. 2003). We then use the radius where the mean density drops below 200 times the critical density of the universe ($r_{vir} \equiv r_{200}$) to measure the halo mass therein ($m_{vir} \equiv m_{200}$). This results in a complete halo catalogue ($n_{\rm halos}$ = 41313) for halos more massive than $2 \times 10^{10} M_\odot h^{-1}$ which have properties typical for this kind of simulation (see Moster et al. 2010 for a detailed analysis of this simulation). In brief, we show the dark matter halo mass function at z=0 and z=2 in Fig. 1 along with the analytical prediction from Sheth et al. (2001) where we find small variations at the high mass end due to the limited boxsize. The corresponding distribution of the dimensionless spin parameter

$$\lambda' \equiv \frac{J}{\sqrt{2} m_{vir} V_c r_{vir}}, \qquad (1)$$

defined by Bullock et al. (2001), is shown in Fig. 2. Here J is the total angular momentum within r_{vir} and V_c is the halo circular velocity $V_c^2 = G m_{vir}/r_{vir}$. The distribution of angular momenta is consistent with previous simulations (Bullock et al. 2001; Vitvitska et al. 2002) and can be fitted with a log-normal distribution

$$P(\lambda') = \frac{0.01}{\lambda' \sqrt{2\pi}\sigma} \exp\left(-\frac{\ln^2(\lambda'/\lambda'_0)}{2\sigma^2}\right) \qquad (2)$$

with best-fit values $\lambda'_0 = 0.038$ and $\sigma = 0.58$.

2.2. *Refined Simulations*

For the higher resolution re-simulations of individual halos we trace all dark matter particles that are closer than $2 \times r_{200}$ to the center of the halo at z=0. Following the halo back in time we include all particles in the tracing process which are within $2 \times r_{200}$ of the halo center at any given snapshot. This ensures that halo encounters during the assembly of the halo of interest are always resolved. We found this to be an efficient mechanism to reduce contamination with massive boundary particles. The traced particles define the region for which we have to generate higher resolution initial conditions. For the cuboid enclosing this region we compute the short wavelength modes of the perturbation spectrum using GRAFIC2 (Bertschinger 2001). Based on the new spectrum we replace the low resolution dark matter particles

TABLE 1
Central Galaxies

ID	m_{200}[a]	r_{200}[b]	m_*[c]	m_{gas}[d]	m_{ins}/m_*[e]	t_*[f]	t_{ins}[g]	t_{acc}[h]	t_{50}[i]	n_{gas}[j]	n_*[k]	n_{halo}[l]
0040	2676	486	36.0	4.13	0.231	10.8	9.90	11.1	2.73	579933	440633	2096930
0069	1775	424	35.6	3.13	0.218	10.8	8.66	11.4	6.37	354378	306742	1378352
0089	1064	358	37.7	2.58	0.163	11.0	9.91	11.2	4.75	214528	182465	826895
0094	1004	351	34.5	3.46	0.258	10.9	9.10	11.6	7.67	210596	164402	780411
0125	917	340	31.2	2.94	0.224	11.1	9.59	11.6	8.31	200865	146889	716832
0162	630	300	26.2	2.64	0.129	10.8	8.49	11.2	2.58	134454	106554	494315
0163	689	309	25.3	1.73	0.150	10.5	9.11	10.8	4.75	139297	119486	536504
0175	699	311	26.5	1.29	0.270	11.3	9.74	11.8	9.56	127745	117170	530274
0190	511	280	22.7	1.71	0.146	10.3	8.39	10.6	3.81	103075	98844	405894
0204	538	285	19.3	1.42	0.156	10.8	8.77	11.2	8.31	102722	99548	419003
0209	595	295	14.4	0.656	0.337	10.9	9.71	11.5	9.26	118459	97601	457580
0215	505	279	19.9	1.14	0.352	11.0	9.93	11.5	8.15	100251	87072	391385
0224	478	274	17.9	2.06	0.200	10.3	7.69	11.0	6.20	89336	91799	373489
0259	437	266	14.3	1.23	0.262	10.9	8.98	11.6	9.72	83945	81751	341491
0300	365	250	13.4	1.63	0.201	10.4	8.64	10.8	5.88	72180	64276	283964
0329	350	247	15.4	0.696	0.341	10.9	9.55	11.6	9.10	65296	63583	270652
0380	328	242	12.3	0.634	0.491	10.9	10.0	11.8	10.6	58842	56464	249316
0408	253	221	12.8	1.90	0.300	10.1	7.09	11.3	8.31	49561	50348	200794
0443	268	226	16.6	1.91	0.277	10.3	6.55	11.7	8.31	50289	52800	210493
0501	230	215	11.7	0.93	0.361	10.8	10.0	11.2	8.79	48521	40463	181178
0549	216	210	8.38	0.450	0.262	10.7	8.71	11.4	9.41	39034	39605	165346
0616	189	201	9.38	0.455	0.367	10.6	9.88	11.0	9.72	34520	37188	147962
0664	179	197	7.48	0.558	0.343	10.7	9.06	11.6	9.41	34393	30862	138039
0721	147	185	9.63	0.629	0.536	8.88	7.07	11.0	6.69	22910	34776	116680
0763	150	186	9.85	0.177	0.197	10.4	9.19	10.8	6.37	25283	34151	119180
0858	139	181	10.3	0.790	0.355	8.92	5.49	10.8	6.69	21022	33759	110365
0908	125	175	9.67	0.708	0.458	8.84	6.55	10.8	7.50	19927	33080	102025
0948	121	173	6.64	0.442	0.308	10.6	9.38	11.2	9.56	22627	23147	94475
0959	120	173	6.05	0.399	0.371	10.1	9.46	10.5	9.41	23591	23027	94670
0977	94.4	159	4.55	0.464	0.496	9.10	7.21	11.0	8.63	16592	20916	75143
1017	106	166	6.39	0.736	0.584	10.0	8.92	11.5	9.87	21049	20634	83999
1061	103	164	5.18	0.439	0.335	9.98	8.72	10.6	8.15	19196	20400	81076
1071	106	166	7.79	0.610	0.317	9.66	7.06	10.9	8.15	18696	24045	84818
1091	112	169	7.53	0.416	0.280	9.24	5.37	10.7	6.20	18487	26210	89119
1167	93.0	159	7.37	0.659	0.331	9.32	5.88	11.0	6.85	15966	22371	75141
1192	78.0	150	4.36	0.157	0.442	10.4	9.54	11.0	9.56	13041	15792	60404
1196	95.4	160	7.73	0.99	0.490	9.23	6.96	11.4	7.67	16839	20987	75883
1646	71.3	145	5.38	0.509	0.480	8.90	6.23	11.4	8.31	11143	16557	56264
1859	70.0	144	4.52	0.340	0.429	9.82	7.86	11.3	9.56	12355	16458	56488

Note. — all masses in units of $10^{10}h^{-1}M_\odot$, timescales in Gyr.
[a]virial mass, [b]virial radius in kpc/h, [c]stellar mass inside r_{10} , [d]gas mass inside r_{10}, [e]ratio of in-situ to ex-situ created stars, [f]mean stellar age , [g]mean stellar age of in-situ created stars, [h]mean stellar age of ex-situ created stars, [i]lookback time where 50 per cent of the final stellar mass is in place, [j]number of gas particles inside r_{200}, [k]number of star particles inside r_{200}, [l]total number of particles inside r_{200}. The horizontal bars indicate the separation into small, intermediate and high mass galaxies used throughout this paper

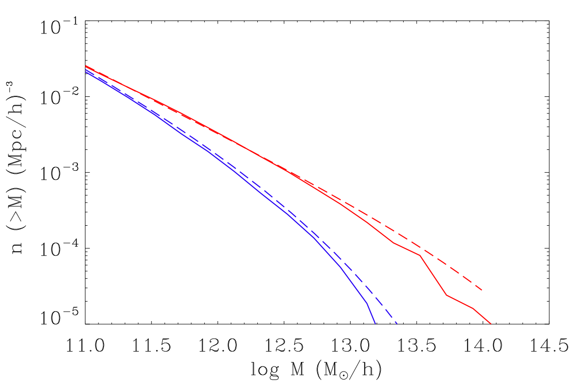

Fig. 1.— Dark matter mass Function (solid) of the $(72h^{-1}Mpc)^3$ box at z=0 (red) and z=2 (blue). The dashed lines show the prediction of Sheth et al. (2001).

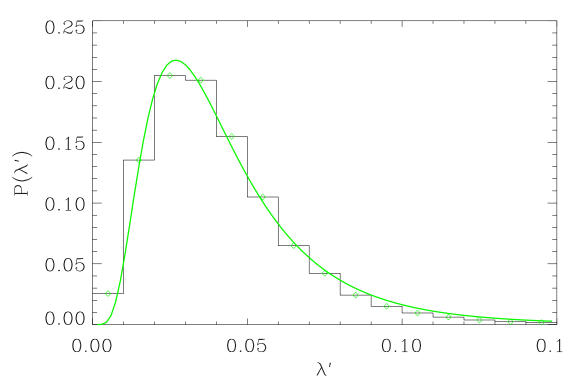

Fig. 2.— Spin parameter distribution for the dark matter box. The green line shows the log-normal-fit with best fit values $\lambda'_0 = 0.038$ and $\sigma = 0.58$.

with dark matter as well as gas particles at higher resolution (Ω_b=0.044, Ω_{dm}=0.216). We only consider coherent regions within the cuboid that actually contain traced particles. Other regions as well as a 'safety margin' of 1Mpc h^{-1} around the high-resolution cuboid are populated with particles from the original initial conditions. To approximate the long range tidal forces, particles from the original simulation being further away from the center are merged, with the particle masses increasing as the square of the distance from the region of interest. By this and the inclusion of periodic boundaries tidal forces from distant regions are accurately included in the computations.

We obtain amoeba shaped initial conditions (see Fig. 3) for which, on average, approximately 30% of the high resolution dark matter particles end up inside the virial radius at redshift $z = 0$ (see Power et al. 2003 and in particular Jenkins 2010 for alternative ways of creating high resolution initial conditions). The particle number in the boundary region is kept low enough to perform the simulations in a reasonable time. For example the most massive halo #0040 which has a total mass m_{200} of $2.7 \times 10^{13} M_{\odot} h^{-1}$ at $z = 0$ took ~ 23000 CPU-hours to evolve (3.8×10^6 high-resolution particles in dark matter and gas each). In the re-simulations the particles in the high resolution regions have a gas and star mass of $m_{*,gas} = 4.2 \times 10^6 M_{\odot} h^{-1}$ (we spawn one star per gas particle) and a dark matter mass of $m_{dm} = 2.5 \times 10^7 M_{\odot} h^{-1}$ which is 8 smaller than in the original simulation. The comoving gravitational softening length for the gas and star particles is 400pc h^{-1} and 890pc h^{-1} for the high resolution dark matter particles, scaled with the square root of the mass ratio (Dehnen 2001). Compared to some other recent cosmological zoom simulations (Scannapieco et al. 2009; Governato et al. 2009; Piontek & Steinmetz 2009; Feldmann et al. 2010) the resolution level of our simulations at $M_{halo} \approx 10^{12} M_{\odot}$ is slightly lower. But while these simulations are limited to a few halos in a small mass range we performed a significantly larger number of re-simulations of halos spanning a mass range of almost two orders of magnitude. The present-day properties of our re-simulated galaxies can be found in Table 1. Finally, we also performed a number of re-simulations at higher resolution, i.e. with particle masses 8 times lower and half the softening length. While increasing resolution can slightly change the individual accretion histories of the galaxies, the global trends found in this paper remain the same.

2.3. *Simulation details*

The simulations presented here have been performed using the parallel TreeSPH code GADGET-2 (Springel 2005) which calculates the gas dynamics using the Lagrangian Smoothed Particle Hydrodynamics technique (SPH, see e.g. Monaghan 1992). The code ensures the conservation of energy and entropy (Springel & Hernquist 2002) and includes star formation and cooling for a primordial composition of hydrogen and helium, where the cooling rates are computed under the assumption that the gas is optically thin and in ionization equilibrium (Katz et al. 1996). Additionally, the simulations include a spatially uniform redshift-dependent UV background radiation field with a modified Haardt & Madau 1996 spectrum, where reionization takes place at $z \approx 6$ (Davé et al. 1999) and the UV background radiation field peaks at $z \approx 2 - 3$. For a recent detailed investigation on the effects of varying the background radiation field on the evolution of galaxies, see e.g. (Hambrick et al. 2010).

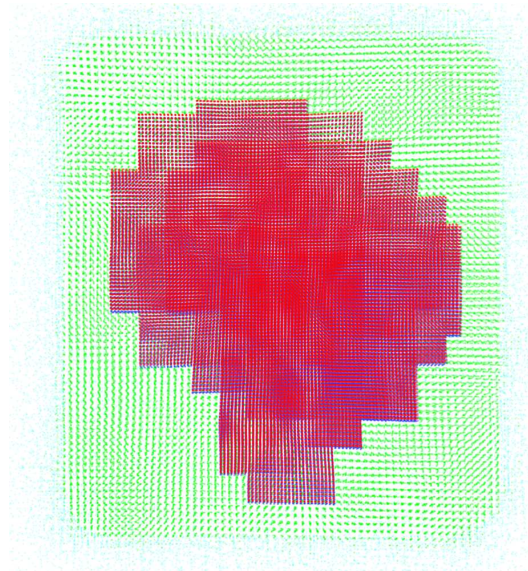

Fig. 3.— Central region of the initial conditions for halo #0408 at z=43. The innermost region consists of the high-resolution gas and dark matter particles (red and blue). The green particles are dark matter particles taken from the original dark-matter-only run. The outermost dark matter particles have increasing mass depending on the distance, with sufficient resolution to represent the long range tidal forces.

For the star formation and feedback prescription we use the self-regulated supernova feedback model of Springel & Hernquist 2003. This models treats the ISM as a two-phase medium (McKee & Ostriker 1977; Johansson & Efstathiou 2006) where clouds of cold gas are embedded in the hot gas phase at pressure equilibrium. Stars are allowed to form out of the cold gas phase if the local density exceeds a threshold value ($n > n_{\rm th} = 0.205 {\rm cm}^{-3}$) which is calculated self-consistently in a way that the equation of state is continuous at the onset of star formation. In this model the star formation rate is set by $d\rho_*/dt = (1 - \beta)\rho_c/t_*$, where β is the mass fraction of massive stars ($> 8M_{\odot}$), ρ_c is the density of cold gas and t_* is the star formation time scale set by $t_* = t_*^0 (n/n_{th})^{-1/2}$. The massive short-lived stars heat up the surrounding gas with an energy input of $10^{51} ergs$ due to supernovae. In order to prevent spurious star formation at high redshift we require an over-density of $\Delta > 55.7$ for star formation to set in.

2.4. *The baryonic mass budget*

Using similar parameters for zoom simulations has been shown to result in galaxies with reasonable present day properties (Naab et al. 2007, 2009; Johansson et al. 2009, 2010 in prep.). However, the employed star formation prescription favors efficient star formation at early times resulting in preferentially spheroidal systems with old stellar populations, due to the strongly self-regulated feedback which does not produce the supernova driven winds. Fig. 4 shows the conversion ef-

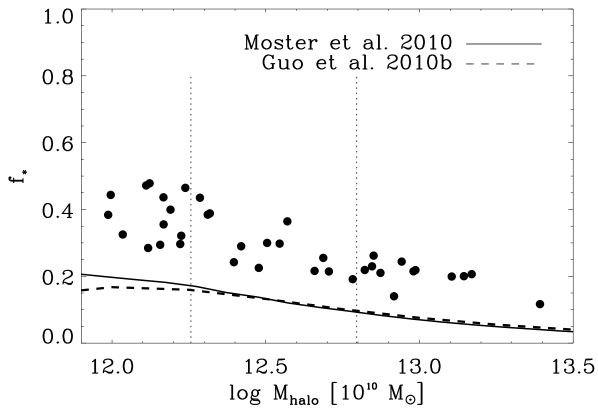

FIG. 4.— Fraction of baryons that is converted into stars at redshift zero. The vertical dotted lines indicate the separation into the different mass bins. The solid black line shows the results of Guo et al. (2010b), the dashed line those of Moster et al. (2010).

ficiency of the simulated galaxies at the present day $f_* = m_*/(f_b * m_{vir,dark})$ where m_* is the stellar mass within 10 % of the virial radius, $f_b = \Omega_b/\Omega_{dm} = 0.20$ is the cosmic baryon fraction and $m_{vir,dark}$ is the dark matter mass within the virial radius of the galaxy. Therefore $f_b * m_{vir,dark}$ is the amount of total baryonic matter available in each halo and f_* the fraction thereof that is converted into stars in the central galaxy. This fraction declines in a roughly linear fashion with the logarithm of the halo mass from $f_* \approx 0.5$ for the smallest halos ($\approx 10^{11.9} M_\odot$) to $f_* \approx 0.15$ for high mass halos ($\gtrsim 10^{13} M_\odot$) , still over-predicting by a factor of 2 the estimation from recent models (see however **?** who find higher efficiencies for high mass galaxies) that are tested by matching observed luminosity functions to simulated halo mass functions (Moster et al. 2010; Guo et al. 2010b; Conroy & Wechsler 2009; Behroozi et al. 2010) or weak lensing observations (Mandelbaum et al. 2006). Note that a Salpeter initial mass function would increase the 'observed' conversion efficiency by approximately a factor of two (**?**).

The physical processes probably responsible for this discrepancy are well studied and it has been argued that feedback from SNII is important for low mass systems (e.g. Larson 1974; Dekel & Silk 1986; Guo et al. 2010a) and feedback from supermassive black holes dominates for high mass systems (Croton et al. 2006; Di Matteo et al. 2008). Although this issue is relatively well understood and many idealized calculations have shown how these feedback processes can expel the baryons from galaxies, there have been only a few high resolution galaxy formation calculations, using cosmological initial conditions, beginning to master the physics well enough to match either the winds seen in forming galaxies or the final metal distribution between galaxies and the IGM (Scannapieco et al. 2008; Sawala et al. 2010). Some other calculations do successfully allow for winds and for the consequences these winds have on the galaxies and the surrounding ISM (Springel & Hernquist 2003; Oppenheimer & Davé 2008; Oppenheimer et al. 2010; Cen & Chisari 2010; Wiersma et al. 2010; McCarthy et al. 2010). Our computations do not generate significant winds at high red-

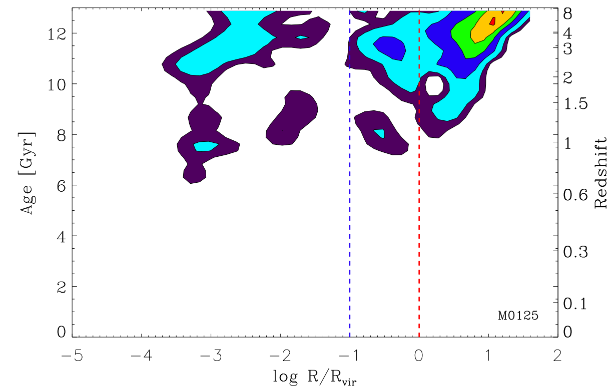

FIG. 5.— Stellar origin diagram for all stars within r_{10} at $z = 0$ in galaxy M0125. Every grey dot indicates the time when a stellar particle was born and the distance, in units of the virial radius of the main galaxy at that time, where it was born. The contours enclose 90% (purple), 80%(turquoise), 60% (blue), 40% (green), 25% (orange) and 10% (red) of the stars, respectively. The blue and red vertical lines show the virial radius and 10% of the virial radius, respectively. There is a clear distinction between stars initially formed in the galaxy and those formed outside the galaxy and are accreted later on (78 percent of all stars).
(Dots excluded for file size reasons)

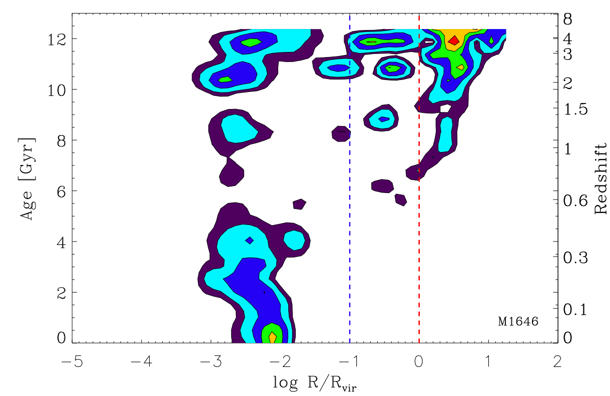

FIG. 6.— Same as Fig. 5 but for the low mass galaxy M1646. There is significant in-situ star formation at the center even at low redshift and significantly less accretion of stars. In this case only 52 per cent of the stars are accreted.
(Dots excluded for file size reasons)

shift (e.g. Steidel et al. 2010) and thus overestimate, by roughly a factor of two, the condensed baryon fraction of massive galaxies (Guo et al. 2010b; Moster et al. 2010). This becomes worse if we extend the sample to lower masses where the halo occupation models predict a sharp drop off the conversion efficiency f_*. This is probably due to the fact that ejective supernovae wind feedback, which is not included in the present study, is most effective in this regime. We are currently working to implement physically valid feedback implementations to address this problem.

3. THE TWO PHASES OF GALAXY FORMATION

The stellar particles ending up in the simulated galaxies at $z = 0$ are of two different origins. Some fraction of the stars are made in-situ, within the galaxies, from accreted gas and some fraction of the stars are made

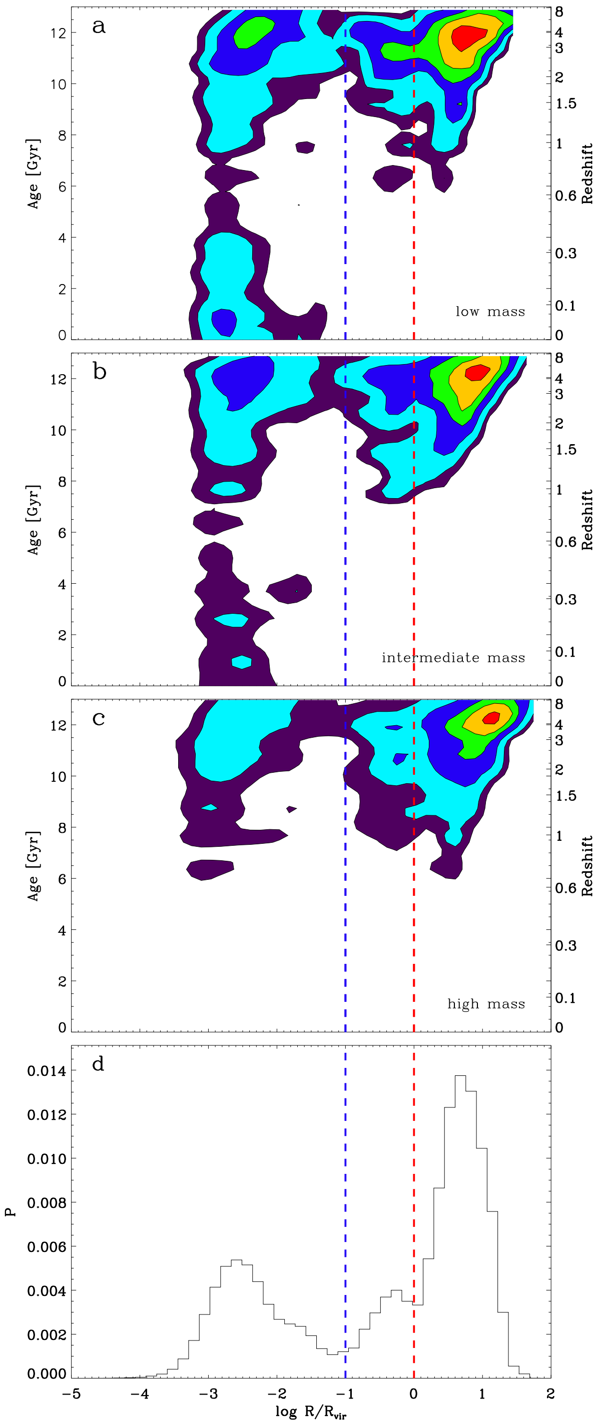

FIG. 7.— Same as Fig. 5 but for all galaxies in low mass halos in the mass range $7.0 \times 10^{11} - 1.3 \times 10^{12} h^{-1} M_\odot$ (panel a), for intermediate halo masses in the range $1.3 \times 10^{12} - 4.5 \times 10^{12} h^{-1} M_\odot$ (panel b), and for all high mass halos with $4.5 \times 10^{12} - 2.7 \times 10^{13} h^{-1} M_\odot$ (panel c). The contours show the same percentiles as in Figs. 5 and 6. The stars form in two phases, either inside r_{10} or outside $r_{\rm vir}$ as can be seen in panel d. Galaxies in low mass halos have ongoing in-situ star formation (see Fig. 10) at relatively high specific rates until the present day, whereas in the highest mass group most star formation is complete by z=2.

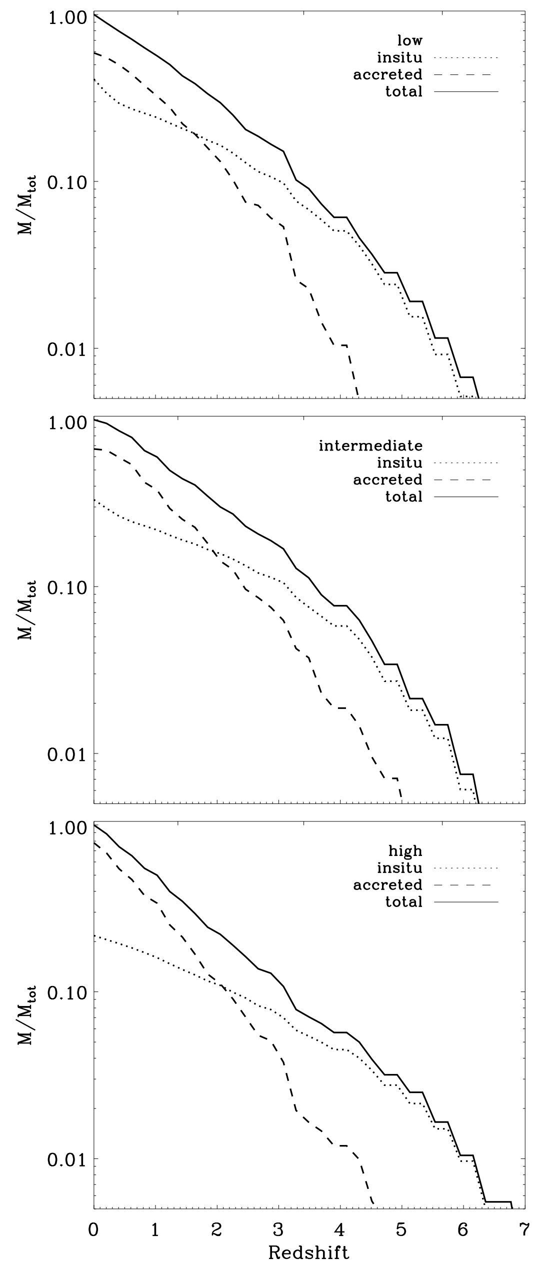

FIG. 8.— Stellar mass assembly histories (solid lines) for low mass (top), intermediate mass (middle) and high mass (bottom) galaxies. The assembly is separated into in-situ stars (dotted line) and ex-situ stars that are accreted onto the galaxy later on (dashed line). The assembly of higher mass galaxies is more dominated by in-situ formation at high redshift, however, the total fraction of accreted stars by z=0 is higher ($\approx 80\%$) for massive systems than for low mass systems ($\approx 60\%$).

ex-situ outside the galaxies and are accreted later on (Naab et al. 2007; Johansson et al. 2009). The relative amount of in-situ and ex-situ stars is found to vary systematically with galaxy mass. Two typical stellar origin diagrams indicating this behavior are shown in Fig. 5 and Fig. 6.

To construct these diagrams we follow every star that ends up within 10% of the present-day virial radius of a simulated galaxy back in time. We use 10% of the virial radius, r_{10}, as a fiducial value for the extent of the stel-

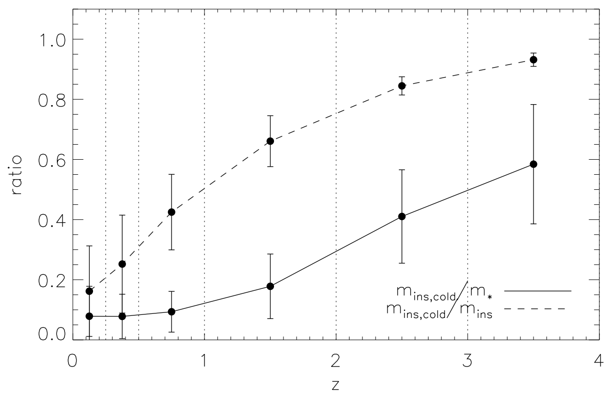

FIG. 9.— Average ratio of in-situ created stars that formed inside the bins indicated by the vertical dotted lines out of gas that was accreted cold to the total mass of in-situ created stars (dashed line). The solid line shows the ratio of the stars created in-situ out of cold gas to the total stellar mass growth, this includes in-situ star formation as well as accretion. The error bars corespond to the 1σ-dispersion.

lar component of a simulated final galaxy inside its dark matter halo. Then we mark the time when a star was born as well as its distance from the galaxy center in units of the virial radius (at this time) with a grey dot. The values are discrete in time representing the discrete snapshots. The contours in these plots encompass the smallest number of bins that include 10, 25, 40, 60, 80 and 90 per cent of the stars, respectively. In Fig.5 we show the stellar origin diagram for a massive system with a halo mass of $\sim 10^{13} M_{\odot} h^{-1}$. At redshifts $z > 2$ there are two separate peaks of star fomation: one inside r_{10}, which is in-situ star formation and another one outside the virial radius of the system at that time. This indicates that a significant fraction of the stars in the present-day galaxy was made outside the galaxy and has been accreted later on. For this system the in-situ star formation decreases towards lower redshifts. Although there is ongoing star formation until z=0 the contribution to the final galaxy is negligible, since the contoured regions include 90 per cent of all stars in the galaxy. For a lower mass system with a halo mass of $7.1 \times 10^{11} M_{\odot} h^{-1}$ the same analysis is shown in Fig. 6. In this case the fraction of stars forming ex-situ is lower and the contoured regions extend up to the present day, i.e. in-situ star formation continues at a significant level towards lower redshift.

In Fig. 7, we have stacked all simulated galaxies of our sample into three mass bins (indicated by the horizontal bars in table 1) with the same number of objects (13), every star particle is weighted according to the total number of stars in its host galaxy, so that every galaxy has an equal weight. The low mass bin contains galaxies with halo masses in the range $7.0 \times 10^{11} - 1.3 \times 10^{12} M_{\odot} h^{-1}$ (panel a), intermediate mass galaxies have $1.3 \times 10^{12} - 4.5 \times 10^{12} M_{\odot} h^{-1}$ (panel b) and high mass galaxies have $4.5 \times 10^{12} - 2.7 \times 10^{13} M_{\odot} h^{-1}$ (panel c). These plots again demonstrate in a more statistical sense that the stars ending up in the final galaxies form in two distinct phases, namely in-situ in the galaxy and ex-situ outside the virial radii of the galaxies (red vertical dashed lines). The spatial division line between these two phases of star formation is at about 10% of the virial radius indicated

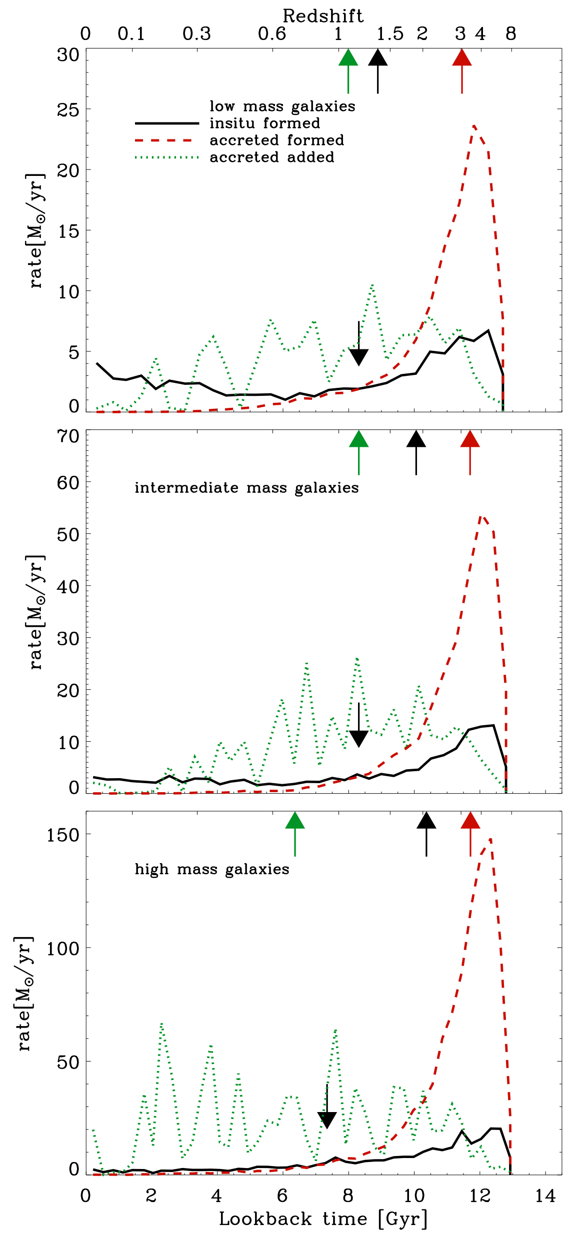

FIG. 10.— Star formation histories for low mass (upper panel), intermediate mass (middle panel) and high mass galaxies (lower panel) for all stars that end up inside the galaxy at $z = 0$. The solid black line shows the formation of the in-situ created stars, the red dashed line the formation of the ex-situ stars and the green dotted line shows the accretion rate of the ex-situ stars onto the galaxy. The arrows on top indicate the time at which half the stars are formed/added. The arrow at the bottom indicates the time at which 50% of the final galaxy mass is assembled.

by the vertical blue dashed lines in Fig. 7. In addition, there is a clear trend that low mass galaxies have relatively more in-situ star formation at low redshift $z < 1$ than higher mass galaxies. For the most massive galaxies the contribution from late in-situ star formation is relatively small. Panel d shows a histogram for the formation radii for all stars in all simulations. For this analysis we use 45 logaritmically evenly spaced bins. We see two peaks, for the in-situ created stars at $\log(r/r_{vir}) \approx -2.5$ and for the ex-situ created stars at $\log(r/r_{vir}) \approx 0.6$, re-

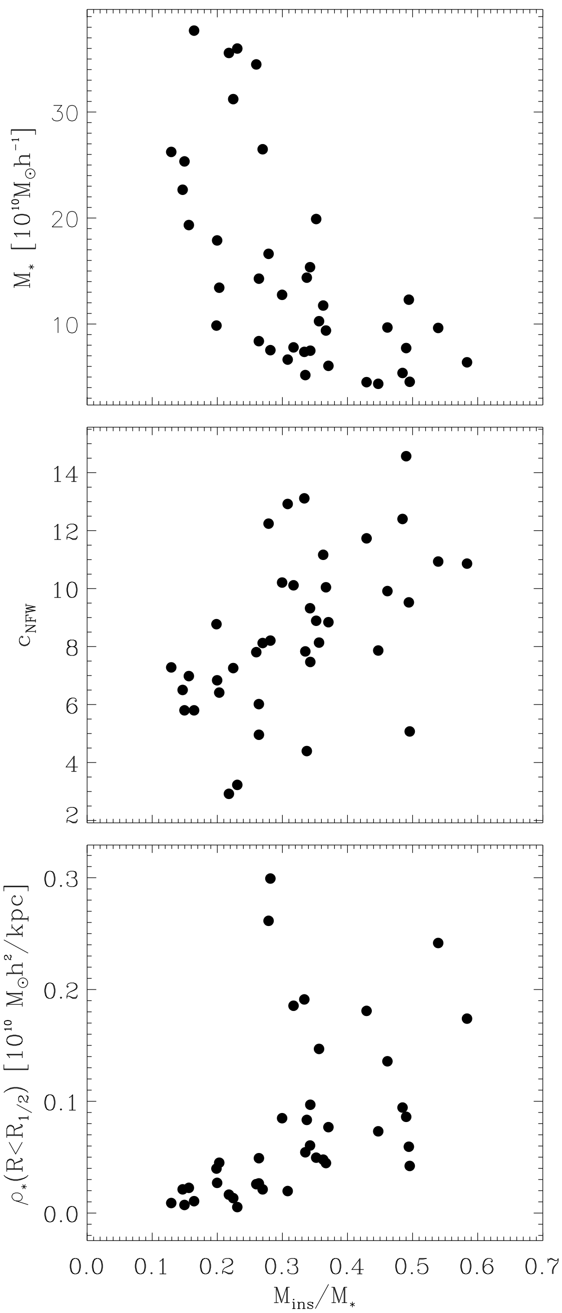

FIG. 11.— From top to bottom: Fraction of in-situ stellar mass vs total stellar mass inside r_{10}, halo concentration and stellar density inside $R_{1/2}$ at $z = 0$. There is a clear trend that galaxies with less in-situ star formation are more massive, have less concentrated halos and lower density central regions.

spectively. A third peak appears between r_{10} and r_{vir} that is due to infalling substructure that is still star-forming.

In Fig. 8 we show the average mass accretion histories for the stellar particles in the three mass bins separated into in-situ and ex-situ/accreted stars depending on whether they have formed inside or outside 10% of the virial radius. The galaxy growth is dominated for all three mass bins by in-situ star formation until $z \approx 2$, when the mass of accreted stars equals the mass of in-situ stars. By $z = 0$ about $41 \pm 9\%$ (we give mean values and the 1σ-dispersion of the 13 galaxies) of the stars in the low mass sample (top panel) have formed in-situ, the rest were accreted. For the intermediate mass galaxies (middle panel) the fraction of in-situ stars is lower than for the low mass sample of $\approx 33 \pm 10\%$, and 67% of the stars were accreted. With $78 \pm 7\%$ the fraction of accreted stars is even higher for the massive galaxies. On average only 22% of the present-day stellar mass is formed in-situ which is the dominant mode until $z \approx 2$ but thereafter contributes very little to the stellar mass growth.

Following Kereš et al. (2005) and Kereš et al. (2009a) we examined whether the gas out of which the in-situ stars are formed in our galaxies was ever heated above $T_{hot} > 2.5 \times 10^5 K$ throughout the simulation. The results can be seen in Fig. 9. The dashed line shows, that up to redshift 2, where in-situ star formation is still dominating over accretion, almost all of the in-situ stars are formed out of gas that was accreted cold. Only at later times ($0 < z < 2$), when stellar accretion is the primary source of stellar mass growth, in-situ stars are forming out of cooling hot halo gas. At lower redshift the contribution of in-situ star formation out of cold flows to the total stellar mass growth becomes almost negligible (dotted line in Fig. 9). The interpretation of the results does not change when we instead of a fixed temperature cut use a temperature threshold related to the current halo virial temperature (see Kereš et al. (2005)). This is in agreement with the previous results of numerical simulations (Kereš et al. 2009a) and analytical predictions (Dekel & Birnboim 2006) that galaxy growth at high redshift ($z \geq 2$) is dominated by cold accretion.

Fig. 10 illustrates the star formation and assembly histories for the galaxies in the three mass bins. The red dashed line shows the archaeological star formation history of the accreted stars computed from the mass weighted ages of the accreted stars at the present day. All curves show a steep increase towards the peak at $z \approx 4$ at values of $\approx 25 M_\odot yr^{-1}$, $\approx 55 M_\odot yr^{-1}$, and $\approx 150 M_\odot yr^{-1}$ for the low, intermediate and massive bin, respectively. This is followed by an approximately exponential decline towards $z = 0$. The red arrow on top indcates the time when half of the accreted stars are formed. In all cases, i.e. at all masses this is at $z \approx 3$. The green dotted line shows when these stars are accreted onto the galaxies. As this happens in mergers, the curves show peaks. On average the rates increase towards $z = 2$ and then stay relatively flat with average rates of $\approx 3.6 M_\odot yr^{-1}$, $\approx 8.2 M_\odot yr^{-1}$, and $\approx 17 M_\odot yr^{-1}$. The green arrow on top indicates when half of the present-day mass in ex-situ stars is accreted onto the galaxies. This happens around z=0.7-1.2 and therefore significantly later than the formation of these stars at z=3-4. The black solid line shows the formation history of the in-situ stars in the galaxies. This is most closely related to the star formation rate that would actually be observed in these galaxies. All curves peak at $z \geq 3.5$ at rates between ≈ 5 and $\approx 20 M_\odot yr^{-1}$. Independent of galaxy mass all rates drop to $\approx 2 - 3 M_\odot yr^{-1}$ at $z = 1$ and stay constant to the present day similarly to the observations of massive galaxies by Juneau et al. (2005). This results in a specific star formation rate of 0.31 ± 0.15, 0.18 ± 0.15 and $0.053 \pm 0.071 \times 10^{-10} yr^{-1}$ for the different mass

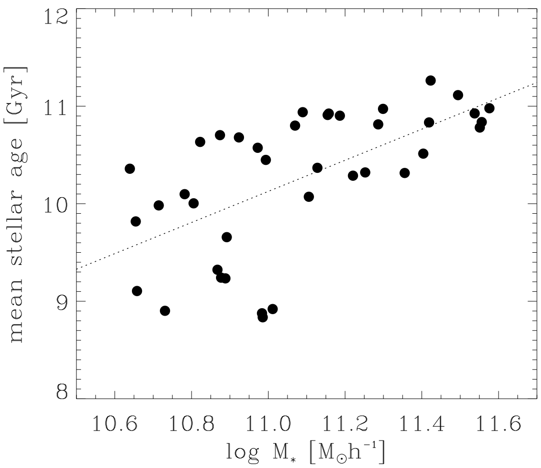

FIG. 12.— Mean age of the stars inside r_{10} as function of galaxy mass. High mass galaxies consist of older stars than the low mass galaxies, recovering the phenomenon usually referred to as 'archaeological downsizing' ($t_{mean} \propto \log M_*^{1.6}$).

bins. According to the definition by Franx et al. 2008 ($SFR/m_* < 0.3/t_{thub}$) the galaxies in the high mass bin would correspond to quiescent galaxies. The time when half of the in-situ stars are formed is indicated by the top black arrows. This changes systematically with galaxy mass from z=1.4 to z=1.9 and z=2.1, i.e. the in-situ component is oldest for the most massive systems. The black arrow at the bottom of the panels indicates the time when half of the final galaxy was assembled. For all galaxies this is around redshift $z \approx 1$. Therefore all galaxies double their mass since then. For low mass systems the low redshift growth is dominated by in-situ formation whereas for high mass systems it is dominated by accretion of small stellar systems (Tiret et al. 2010).

In summary, at high redshift the assembly of galaxies at all masses is dominated by in-situ star formation fed by cold flows. The larger the galaxy mass the smaller is the late contribution of in-situ star formation. At low redshift, $z < 1$, the growth of low mass galaxies continues by in-situ star formation and stellar accretion whereas, massive galaxies grow predominantly by accretion of ex-situ stars (see e.g. Feldmann et al. 2010; Naab et al. 2009).

In Fig. 11 we show interesting correlations of galaxy and halo properties with the fraction of in-situ stars indicating that this quantity is an important tracer of galaxy assembly. Essentially, this ratio, m_{ins}/m_*, is a dimensionless measure for the degree to which the galaxy was formed by a dissipational versus a dissipationless process (Lackner & Ostriker 2010). The fraction of the stellar galaxy mass formed in-situ m_{ins}/m_* is highest, up to 60%, for low mass galaxies and declines almost linearly (despite some scatter) with increasing galaxy mass down to $\approx 13\%$ for the most massive systems in our simulations which are the central galaxies of massive groups (top panel of Fig. 11). This trend is very similar to semi-analytical predictions (Khochfar & Silk 2006a) and constraints based on halo occupation models combined with isolated merger simulations (**?**). In the central panel of Fig. 11 we show the fraction of in-situ mass versus the concentration parameter c of the dark halo which is defined as the ratio between r_{200} and r_s, where r_s is the scale radius for an NFW fit (Navarro et al. 1997) of the density profile:

$$\rho(r) = \frac{\delta_c \rho_{crit}}{(r/r_s)(1 + r/r_s)^2} \tag{3}$$

For the fit we binned the halo into 32 spherical shells equally spaced in $log_{10}(r)$ between r_{200} and $log_{10}(r/r_{200}) = -2.5$ similar to Grossi & Springel (2009). We see a continuous change of the dark matter halo concentration. As expected from the effect of adiabatic contraction galaxies with significant in-situ star formation, i.e. more dissipation, live in more concentrated halos (Blumenthal et al. 1986; Dubinski 1994; Jesseit et al. 2002; Debattista et al. 2008; Gnedin et al. 2004; Abadi et al. 2010; Auger et al. 2010). The concentration of more massive halos does not increase significantly as the matter is added predominantly in stellar form and cannot dissipate (see e.g. Johansson et al. 2009 and references therein), i.e. the adiabatic contraction approximation cannot be applied for massive galaxies. The bottom panel in Fig. 11 shows the stellar density inside the spherical half-mass radius versus the ratio of in-situ created stars of the galaxies. The two properties are correlated in the sense that galaxies with a large fraction of accreted stars have lower central densities, a well known property of elliptical galaxies (e.g. Bender et al. 1992).

Fig. 10 gives a clue to the paradox of 'downsizing'. The initial expectation was that in a hierarchical universe, since more massive halos statistically are formed later than less massive ones, the same should be true of galaxies. But we know that this is not true observationally (Nelan et al. 2005), giant ellipticals are older - not younger - than lower mass systems (see e.g. Thomas et al. 2005). Our simulations give the same result as can be seen from Fig. 12, the most massive systems are made out of the oldest stars. The inclusion of galactic winds would probably lead to less efficient star formation at high redshifts and leave more gas for late in-situ star formation especially in the lower mass systems, rendering these galaxies even younger. This would lead to an even steeper relation than the one shown in Fig. 12. The explanation of the paradox is obvious: The accreted stars are typically made in smaller systems and these small systems are in fact made at early times (dashed red curves in Fig. 10). Massive galaxies are more dominated by the accreted stars and so by z=0 they contain primarily old stars, although the galaxies themselves are assembled late. De Lucia et al. 2006 obtain the same result with their semi-analytic model. This way the expectation from hierarchical structure formation is satisfied. Both our simulations and the observations of van Dokkum et al. (2008) agree: even at late times massive galaxies continue to grow in mass and size.

4. GALAXY SIZES

The left panel of Fig. 13 shows the present-day spherical half-mass radius for the different components of our galaxies. The size of the in-situ component shows a very weak trend with galaxy mass. For the low mass galaxies the half-mass radii of the in-situ and the accreted stars are of similar size. While the in-situ component does not get larger than $\approx 3\text{kpc}\,h^{-1}$, the half-mass radius of the accreted stars is strongly increasing with galaxy mass

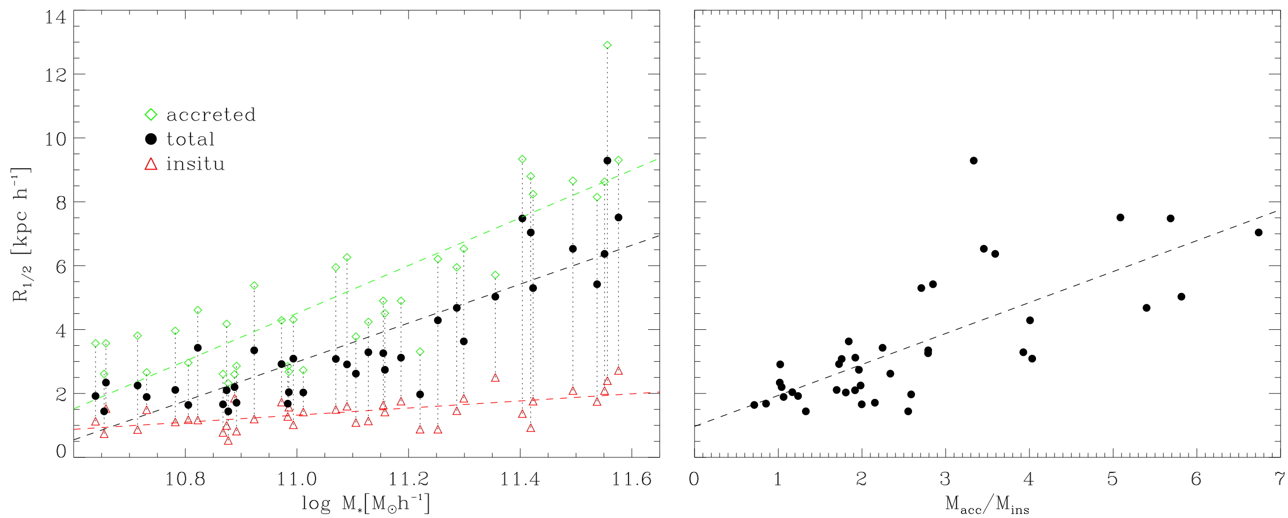

FIG. 13.— *Left panel:* Stellar mass inside 10% of the virial radius vs. spherical half-mass radius of accreted (green diamonds), in-situ (black triangles) and all stars (red squares), respectively. The dashed lines show the results of a linear fit for the respective components ($r_{1/2} \propto \log M_*^{\alpha}$, with $\alpha = 7.5$, 6.1 and 1.1 for the accreted, total and in-situ stars, respectively). While the half-mass radius of the accreted stars strongly increases with mass, the half-mass radius of the in-situ formed stars shows only a weak dependence on galaxy mass. The mass-size relation is driven by the by the accreted stars. *Right panel:* This plot shows the spherical half-mass radii of the galaxies as a function of the ratio of accreted to in-situ created stars. The size increase of the galaxies is roughly linear dependent on this ratio ($r_{1/2} \propto 0.97 * M_{acc}/M_{ins}$).

and since the fraction of accreted stars rises with galaxy mass as well, the global half-mass radius of the galaxies follows this trend. In our simulations the majority of the in-situ created stars are formed in the bulges of the galaxies. Stronger feedback mechanism would probably lead to more star formation in galactic disks resulting in larger radii of the in-situ component. The half-mass radius of the accreted stars should not be affected by this. The right panel of Fig. 13 shows the galaxy radii versus the ratio of accreted to in-situ created stars. We find an almost linear trend. Fig. 13 shows, that stellar accretion is the dominant mechanism for the size growth of massive galaxies. For most of our systems the accretion of stars is significant at low redshifts, as seen in Fig. 10, especially for the high mass galaxies. Half of the total accreted stellar mass is added to the galaxies between redshift one and the present day which leads to considerable size increase at late times. Consistent with this pictures are the observations from e.g. van Dokkum et al. (2008) and others that show a significant growth between redshift $z = 3$ and $z = 0$ for quiescent early type galaxies. A detailed analysis of this effect will be presented separately. We give, in Naab et al. (2009) a simple argument based on the virial theorem showing how late accretion of low mass satellites ('minor mergers') will lead to the rapid growth in galactic size.

5. SUMMARY AND DISCUSSION

We present results from 39 cosmological re-simulations of dark matter halos including gas and star formation covering a mass range of almost two orders of magnitude in virial mass. In the study presented here we used the simulations to investigate fundamental formation and assembly processes, i.e. how and when do galaxies get their gas and stars, and how does this influence the present day galaxy properties.

We have shown that it can be useful, at a very basic level, to distinguish between stars that are created inside the galaxies themselves (in-situ) and those that are created outside (ex-situ) and are accreted later on. The division into these two separate phases is quite clean (see Fig. 7) with the in-situ stars typically formed closer than $r/r_{vir} \sim 10^{-1}$, i.e. within the galaxy, and the ex-situ stars formed outside the galaxy at $r/r_{vir} \sim 10^{0.5}$ to 10. Independent of galaxy mass we find that the formation of the accreted stars peaks at redshift $z \approx 4$. The in-situ star formation as well has an early peak but extends over a longer period of time. The ratio of stars that are created in-situ to the accreted stars, however varies strongly for galaxies of different masses. We find that for massive galaxies ($\sim 1.9 - 3.6 \times 10^{11} h^{-1} M_\odot$) the contribution of in-situ and accreted stars becomes comparable early ($z \approx 2$) and the accreted stars can account for up to 87% of the final stellar mass. The lower mass galaxies ($\sim 4 - 10 \times 10^{10} h^{-1} M_\odot$) still can have a high fraction of in-situ formed stars up to 60% at the present day. They show a significant amount of in-situ star formation throughout the whole simulation time. The large difference in time when those accreted stars are actually formed and when they are finally assimilated by their host, together with the trend shown of the ratio of in-situ formed stars explains the phenomenon of 'downsizing' (see also (De Lucia et al. 2006) for semi-analytical simulations). The more massive galaxies consist mainly of accreted and therefore old stars leading to the dependence of mean stellar age to galaxy mass shown in Fig. 12. The massive galaxies in our sample assemble about half their mass below a redshift of z=1. This mass increase, caused by stellar accretion and merging, is not accompanied by significant star formation, can be a significant contribution to the observed increase of stellar mass in the early-type galaxy population since z=1 (see e.g. Brown et al. 2007; Faber et al. 2007).

We find that the accreted stars are primarily responsi-

TABLE 2
The assembly of stars in massive galaxies

	In-situ	Accreted
Epoch	$6 \gtrsim z \gtrsim 2$	$3 \gtrsim z > 0$
Baryonic mass source	cold gas flows	minor & major mergers
Size of region	$r_{1/2} \approx 2$kpc	$r_{1/2} \approx 7$kpc
Energetics	Dissipational	Conservative

ble for the low redshift size increase in massive galaxies (see e.g. Hyde & Bernardi 2009). When looking at the half-mass radii of the galaxies and the half-mass radii of the in-situ created and accreted components, we find that the half-mass radius of the in-situ created stars is only weakly dependent on the galaxy mass and is quite small ($\lesssim 3$kpc h^{-1}). This component forms at redshift $z > 2$ and makes the compact cores of the galaxies (see e.g. van Dokkum et al. 2008 and references therein). The larger sizes of galaxies with larger mass are mainly due to the accreted stars creating an outer envelope with half-mass radii exceeding 8kpc h^{-1}.

Our simulations overestimate the stellar mass of the galaxies by roughly a factor of 2. This is probably due to the lack of ejective and preventive feedback mechanism in our simulations. The stars that are accreted as well as the early formed in-situ stars are generated in small systems where winds are most effective and lead to lower star formation rates and therefore lower accretion rates at lower redshifts. The late in-situ star formation should be diminished by AGN feedback particularly in the massive systems. It will be worthwhile to investigate whether and how the inclusion of those processes could influence the presented balance of in-situ star formation to stellar accretion.

The description of galaxy formation as a two phase process followed in a seemingly natural way from our detailed hydro simulations and is organized into a coherent scheme in Table 2. It is not intended as a rival to other ways of seeing galaxy formation but rather as a framework within which the physical processes can be understood in a straightforward way. Early, in-situ star formation is clearly similar to that resulting from the 'cold flow' picture (Dekel et al. 2009a; Kereš et al. 2005) or the earlier descriptive term 'dissipative collapse'. In fact the in-situ phase bears an uncanny resemblance to the 'monolithic collapse' model (Eggen et al. 1962; Partridge & Peebles 1967; Larson 1969; Searle et al. 1973; Larson 1975). The late assembly phase of massive galaxies has many aspects similar to the 'dry merger' paradigm investigated by many authors (Khochfar & Burkert 2003; Khochfar & Silk 2006b; Naab et al. 2006; van der Wel et al. 2009; Bezanson et al. 2009; Nipoti et al. 2009b) with the added qualification that most of the accreted stellar systems are low in mass compared to the final assembled i.e. minor mergers dominate. There appears to be recent archaeological (Coccato et al. 2010) and direct observational for this scenario. van Dokkum et al. (2010) conclude that massive compact galaxies at z=2 (the end of the in-situ phase) have increased their mass at radii $r > 5kpc$ by a factor of ≈ 4 since z=2 with the mass at smaller radii being essentially unchanged.

We thank the referee for valuable comments on the paper. We are grateful to S. D. M. White, S. Faber, P. van Dokkum, M. Kriek , C. Conroy and M. Franx for helpful discussions on the manuscript. The simulation were partly performed at the Princeton PICSciE HPC center. This research was supported by the DFG cluster of excellence 'Origin and Structure of the Universe'.

REFERENCES

Abadi, M. G., Navarro, J. F., Fardal, M., Babul, A., & Steinmetz, M. 2010, MNRAS, 847
Abadi, M. G., Navarro, J. F., Steinmetz, M., & Eke, V. R. 2003, ApJ, 597, 21
Agertz, O., Teyssier, R., & Moore, B. 2010, ArXiv e-prints, 1004.0005
Auger, M. W., Treu, T., Gavazzi, R., Bolton, A. S., Koopmans, L. V. E., & Marshall, P. J. 2010, ArXiv e-prints, 1007.2409
Behroozi, P. S., Conroy, C., & Wechsler, R. H. 2010, ApJ, 717, 379
Bender, R., Burstein, D., & Faber, S. M. 1992, ApJ, 399, 462
Bertschinger, E. 1995, ArXiv Astrophysics e-prints, 9506070
—. 2001, ApJS, 137, 1
Bezanson, R., van Dokkum, P. G., Tal, T., Marchesini, D., Kriek, M., Franx, M., & Coppi, P. 2009, ApJ, 697, 1290
Blumenthal, G. R., Faber, S. M., Flores, R., & Primack, J. R. 1986, ApJ, 301, 27
Brown, M. J. I., Dey, A., Jannuzi, B. T., Brand, K., Benson, A. J., Brodwin, M., Croton, D. J., & Eisenhardt, P. R. 2007, ApJ, 654, 858
Bullock, J. S., Dekel, A., Kolatt, T. S., Kravtsov, A. V., Klypin, A. A., Porciani, C., & Primack, J. R. 2001, ApJ, 555, 240
Cen, R. & Chisari, N. E. 2010, ArXiv e-prints, 1005.1451
Cen, R. & Ostriker, J. P. 1999, ApJ, 514, 1
Coccato, L., Gerhard, O., & Arnaboldi, M. 2010, MNRAS, L97+
Conroy, C. & Wechsler, R. H. 2009, ApJ, 696, 620
Croton, D. J., Springel, V., White, S. D. M., De Lucia, G., Frenk, C. S., Gao, L., Jenkins, A., Kauffmann, G., Navarro, J. F., & Yoshida, N. 2006, MNRAS, 365, 11
Davé, R., Hernquist, L., Katz, N., & Weinberg, D. H. 1999, ApJ, 511, 521
De Lucia, G., Springel, V., White, S. D. M., Croton, D., & Kauffmann, G. 2006, MNRAS, 366, 499
Debattista, V. P., Moore, B., Quinn, T., Kazantzidis, S., Maas, R., Mayer, L., Read, J., & Stadel, J. 2008, ApJ, 681, 1076
Dehnen, W. 2001, MNRAS, 324, 273
Dekel, A. & Birnboim, Y. 2006, MNRAS, 368, 2
Dekel, A., Birnboim, Y., Engel, G., Freundlich, J., Goerdt, T., Mumcuoglu, M., Neistein, E., Pichon, C., Teyssier, R., & Zinger, E. 2009a, Nature, 457, 451
Dekel, A., Sari, R., & Ceverino, D. 2009b, ApJ, 703, 785
Dekel, A. & Silk, J. 1986, ApJ, 303, 39
Di Matteo, T., Colberg, J., Springel, V., Hernquist, L., & Sijacki, D. 2008, ApJ, 676, 33
Dubinski, J. 1994, ApJ, 431, 617
Eggen, O. J., Lynden-Bell, D., & Sandage, A. R. 1962, ApJ, 136, 748

Faber, S. M., Willmer, C. N. A., Wolf, C., Koo, D. C., Weiner, B. J., Newman, J. A., Im, M., Coil, A. L., Conroy, C., Cooper, M. C., Davis, M., Finkbeiner, D. P., Gerke, B. F., Gebhardt, K., Groth, E. J., Guhathakurta, P., Harker, J., Kaiser, N., Kassin, S., Kleinheinrich, M., Konidaris, N. P., Kron, R. G., Lin, L., Luppino, G., Madgwick, D. S., Meisenheimer, K., Noeske, K. G., Phillips, A. C., Sarajedini, V. L., Schiavon, R. P., Simard, L., Szalay, A. S., Vogt, N. P., & Yan, R. 2007, ApJ, 665, 265
Feldmann, R., Carollo, C. M., Mayer, L., Renzini, A., Lake, G., Quinn, T., Stinson, G. S., & Yepes, G. 2010, ApJ, 709, 218
Förster Schreiber, N. M., Genzel, R., Bouché, N., Cresci, G., Davies, R., Buschkamp, P., Shapiro, K., Tacconi, L. J., Hicks, E. K. S., Genel, S., Shapley, A. E., Erb, D. K., Steidel, C. C., Lutz, D., Eisenhauer, F., Gillessen, S., Sternberg, A., Renzini, A., Cimatti, A., Daddi, E., Kurk, J., Lilly, S., Kong, X., Lehnert, M. D., Nesvadba, N., Verma, A., McCracken, H., Arimoto, N., Mignoli, M., & Onodera, M. 2009, ApJ, 706, 1364
Förster Schreiber, N. M., Genzel, R., Lehnert, M. D., Bouché, N., Verma, A., Erb, D. K., Shapley, A. E., Steidel, C. C., Davies, R., Lutz, D., Nesvadba, N., Tacconi, L. J., Eisenhauer, F., Abuter, R., Gilbert, A., Gillessen, S., & Sternberg, A. 2006, ApJ, 645, 1062
Franx, M., van Dokkum, P. G., Schreiber, N. M. F., Wuyts, S., Labbé, I., & Toft, S. 2008, ApJ, 688, 770
Genzel, R., Tacconi, L. J., Eisenhauer, F., Förster Schreiber, N. M., Cimatti, A., Daddi, E., Bouché, N., Davies, R., Lehnert, M. D., Lutz, D., Nesvadba, N., Verma, A., Abuter, R., Shapiro, K., Sternberg, A., Renzini, A., Kong, X., Arimoto, N., & Mignoli, M. 2006, Nature, 442, 786
Gnedin, O. Y., Kravtsov, A. V., Klypin, A. A., & Nagai, D. 2004, ApJ, 616, 16
Governato, F., Brook, C., Mayer, L., Brooks, A., Rhee, G., Wadsley, J., Jonsson, P., Willman, B., Stinson, G., Quinn, T., & Madau, P. 2010, Nature, 463, 203
Governato, F., Brook, C. B., Brooks, A. M., Mayer, L., Willman, B., Jonsson, P., Stilp, A. M., Pope, L., Christensen, C., Wadsley, J., & Quinn, T. 2009, MNRAS, 398, 312
Governato, F., Willman, B., Mayer, L., Brooks, A., Stinson, G., Valenzuela, O., Wadsley, J., & Quinn, T. 2007, MNRAS, 374, 1479
Grossi, M. & Springel, V. 2009, MNRAS, 394, 1559
Guo, Q., White, S., Boylan-Kolchin, M., De Lucia, G., Kauffmann, G., Lemson, G., Li, C., Springel, V., & Weinmann, S. 2010a, ArXiv e-prints
Guo, Q., White, S., Li, C., & Boylan-Kolchin, M. 2010b, MNRAS, 404, 1111
Haardt, F. & Madau, P. 1996, ApJ, 461, 20
Hambrick, D. C., Ostriker, J. P., Johansson, P. H., & Naab, T. 2010, ArXiv e-prints, 1009.6005
Hopkins, P. F., Bundy, K., Croton, D., Hernquist, L., Keres, D., Khochfar, S., Stewart, K., Wetzel, A., & Younger, J. D. 2009, ArXiv e-prints, 0906.5357
Hopkins, P. F., Bundy, K., Hernquist, L., Wuyts, S., & Cox, T. J. 2010, MNRAS, 401, 1099
Hyde, J. B. & Bernardi, M. 2009, MNRAS, 394, 1978
Jenkins, A. 2010, MNRAS, 403, 1859
Jesseit, R., Naab, T., & Burkert, A. 2002, ApJ, 571, L89
Johansson, P. H. & Efstathiou, G. 2006, MNRAS, 371, 1519
Johansson, P. H., Naab, T., & Ostriker, J. P. 2009, ApJ, 697, L38
Joung, M. R., Cen, R., & Bryan, G. L. 2009, ApJ, 692, L1
Juneau, S., Glazebrook, K., Crampton, D., McCarthy, P. J., Savaglio, S., Abraham, R., Carlberg, R. G., Chen, H., Le Borgne, D., Marzke, R. O., Roth, K., Jørgensen, I., Hook, I., & Murowinski, R. 2005, ApJ, 619, L135
Katz, N., Weinberg, D. H., & Hernquist, L. 1996, ApJS, 105, 19
Kauffmann, G., Colberg, J. M., Diaferio, A., & White, S. D. M. 1999, MNRAS, 303, 188
Kereš, D., Katz, N., Davé, R., Fardal, M., & Weinberg, D. H. 2009a, MNRAS, 396, 2332
Kereš, D., Katz, N., Fardal, M., Davé, R., & Weinberg, D. H. 2009b, MNRAS, 395, 160
Kereš, D., Katz, N., Weinberg, D. H., & Davé, R. 2005, MNRAS, 363, 2
Khochfar, S. & Burkert, A. 2003, ApJ, 597, L117
Khochfar, S. & Silk, J. 2006a, ApJ, 648, L21
—. 2006b, MNRAS, 370, 902
Komatsu, E., Smith, K. M., Dunkley, J., Bennett, C. L., Gold, B., Hinshaw, G., Jarosik, N., Larson, D., Nolta, M. R., Page, L., Spergel, D. N., Halpern, M., Hill, R. S., Kogut, A., Limon, M., Meyer, S. S., Odegard, N., Tucker, G. S., Weiland, J. L., Wollack, E., & Wright, E. L. 2010, ArXiv e-prints, 1001.4538
Kriek, M., van der Wel, A., van Dokkum, P. G., Franx, M., & Illingworth, G. D. 2008, ApJ, 682, 896
Lackner, C. N. & Ostriker, J. P. 2010, ApJ, 712, 88
Larson, R. B. 1969, MNRAS, 145, 405
—. 1974, MNRAS, 169, 229
—. 1975, MNRAS, 173, 671
Mandelbaum, R., Seljak, U., Kauffmann, G., Hirata, C. M., & Brinkmann, J. 2006, MNRAS, 368, 715
Marchesini, D., van Dokkum, P. G., Förster Schreiber, N. M., Franx, M., Labbé, I., & Wuyts, S. 2009, ApJ, 701, 1765
McCarthy, I. G., Schaye, J., Ponman, T. J., Bower, R. G., Booth, C. M., Dalla Vecchia, C., Crain, R. A., Springel, V., Theuns, T., & Wiersma, R. P. C. 2010, MNRAS, 740
McKee, C. F. & Ostriker, J. P. 1977, ApJ, 218, 148
Meza, A., Navarro, J. F., Abadi, M. G., & Steinmetz, M. 2005, MNRAS, 359, 93
Meza, A., Navarro, J. F., Steinmetz, M., & Eke, V. R. 2003, ApJ, 590, 619
Monaghan, J. J. 1992, ARA&A, 30, 543
Moster, B. P., Somerville, R. S., Maulbetsch, C., van den Bosch, F. C., Macciò, A. V., Naab, T., & Oser, L. 2010, ApJ, 710, 903
Naab, T., Johansson, P. H., & Ostriker, J. P. 2009, ApJ, 699, L178
Naab, T., Johansson, P. H., Ostriker, J. P., & Efstathiou, G. 2007, ApJ, 658, 710
Naab, T., Khochfar, S., & Burkert, A. 2006, ApJ, 636, L81
Nagamine, K., Cen, R., Hernquist, L., Ostriker, J. P., & Springel, V. 2005, ApJ, 627, 608
Nagamine, K., Ostriker, J. P., Fukugita, M., & Cen, R. 2006, ApJ, 653, 881
Navarro, J. F., Frenk, C. S., & White, S. D. M. 1997, ApJ, 490, 493
Nelan, J. E., Smith, R. J., Hudson, M. J., Wegner, G. A., Lucey, J. R., Moore, S. A. W., Quinney, S. J., & Suntzeff, N. B. 2005, ApJ, 632, 137
Nipoti, C., Treu, T., Auger, M. W., & Bolton, A. S. 2009a, ApJ, 706, L86
Nipoti, C., Treu, T., & Bolton, A. S. 2009b, ApJ, 703, 1531
Oppenheimer, B. D. & Davé, R. 2008, MNRAS, 387, 577
Oppenheimer, B. D., Davé, R., Kereš, D., Fardal, M., Katz, N., Kollmeier, J. A., & Weinberg, D. H. 2010, MNRAS, 860
Partridge, R. B. & Peebles, P. J. E. 1967, ApJ, 147, 868
Pettini, M., Shapley, A. E., Steidel, C. C., Cuby, J., Dickinson, M., Moorwood, A. F. M., Adelberger, K. L., & Giavalisco, M. 2001, ApJ, 554, 981
Piontek, F. & Steinmetz, M. 2009, ArXiv e-prints, 0909.4167
Power, C., Navarro, J. F., Jenkins, A., Frenk, C. S., White, S. D. M., Springel, V., Stadel, J., & Quinn, T. 2003, MNRAS, 338, 14
Sawala, T., Scannapieco, C., Maio, U., & White, S. 2010, MNRAS, 402, 1599
Scannapieco, C., Tissera, P. B., White, S. D. M., & Springel, V. 2008, MNRAS, 389, 1137
Scannapieco, C., White, S. D. M., Springel, V., & Tissera, P. B. 2009, MNRAS, 396, 696
Schaye, J., Dalla Vecchia, C., Booth, C. M., Wiersma, R. P. C., Theuns, T., Haas, M. R., Bertone, S., Duffy, A. R., McCarthy, I. G., & van de Voort, F. 2009, ArXiv e-prints
—. 2010, MNRAS, 402, 0909.5196
Searle, L., Sargent, W. L. W., & Bagnuolo, W. G. 1973, ApJ, 179, 427
Sheth, R. K., Mo, H. J., & Tormen, G. 2001, MNRAS, 323, 1
Somerville, R. S. & Primack, J. R. 1999, MNRAS, 310, 1087
Sommer-Larsen, J., Götz, M., & Portinari, L. 2003, ApJ, 596, 47
Spergel, D. N., Bean, R., Doré, O., Nolta, M. R., Bennett, C. L., Dunkley, J., Hinshaw, G., Jarosik, N., Komatsu, E., Page, L., Peiris, H. V., Verde, L., Halpern, M., Hill, R. S., Kogut, A., Limon, M., Meyer, S. S., Odegard, N., Tucker, G. S., Weiland, J. L., Wollack, E., & Wright, E. L. 2007, ApJS, 170, 377
Springel, V. 2005, MNRAS, 364, 1105
Springel, V. & Hernquist, L. 2002, MNRAS, 333, 649
—. 2003, MNRAS, 339, 289

Springel, V., White, S. D. M., Jenkins, A., Frenk, C. S., Yoshida, N., Gao, L., Navarro, J., Thacker, R., Croton, D., Helly, J., Peacock, J. A., Cole, S., Thomas, P., Couchman, H., Evrard, A., Colberg, J., & Pearce, F. 2005, Nature, 435, 629
Steidel, C. C., Adelberger, K. L., Giavalisco, M., Dickinson, M., & Pettini, M. 1999, ApJ, 519, 1
Steidel, C. C., Erb, D. K., Shapley, A. E., Pettini, M., Reddy, N., Bogosavljević, M., Rudie, G. C., & Rakic, O. 2010, ApJ, 717, 289
Thomas, D., Maraston, C., Bender, R., & de Oliveira, C. M. 2005, ApJ, 621, 673
Tiret, O., Salucci, P., Bernardi, M., Maraston, C., & Pforr, J. 2010, ArXiv e-prints, 1009.5185
Trujillo, I., Conselice, C. J., Bundy, K., Cooper, M. C., Eisenhardt, P., & Ellis, R. S. 2007, MNRAS, 382, 109
van der Wel, A., Bell, E. F., van den Bosch, F. C., Gallazzi, A., & Rix, H. 2009, ApJ, 698, 1232
van Dokkum, P. G., Franx, M., Kriek, M., Holden, B., Illingworth, G. D., Magee, D., Bouwens, R., Marchesini, D., Quadri, R., Rudnick, G., Taylor, E. N., & Toft, S. 2008, ApJ, 677, L5
van Dokkum, P. G., Whitaker, K. E., Brammer, G., Franx, M., Kriek, M., Labbé, I., Marchesini, D., Quadri, R., Bezanson, R., Illingworth, G. D., Muzzin, A., Rudnick, G., Tal, T., & Wake, D. 2010, ApJ, 709, 1018
Vitvitska, M., Klypin, A. A., Kravtsov, A. V., Wechsler, R. H., Primack, J. R., & Bullock, J. S. 2002, ApJ, 581, 799
Wiersma, R. P. C., Schaye, J., Dalla Vecchia, C., Booth, C. M., Theuns, T., & Aguirre, A. 2010, ArXiv e-prints, 1005.3921
Zolotov, A., Willman, B., Brooks, A. M., Governato, F., Hogg, D. W., Shen, S., & Wadsley, J. 2010, ApJ, 721, 738